

1 Sensitivity study of the Regional Climate Model RegCM4 2 to different convective schemes over West Africa

3
4 Brahim KONÉ¹, Arona DIEDHIOU^{1, 2}, N'datchoh Evelyne TOURÉ¹, Mouhamadou Bamba
5 SYLLA³, Filippo GIORGI⁴, Sandrine ANQUETIN², Adama BAMBA¹, Adama DIAWARA¹,
6 Arsene Toka KOBEA¹

7
8 ¹LAPAMF, Université Félix Houphouët Boigny, Abidjan, Côte d'Ivoire

9 ²Univ. Grenoble Alpes, IRD, CNRS, Grenoble INP, IGE, F-38000 Grenoble, France

10 ³WASCAL Centre of Competence, Ouagadougou, Burkina Faso

11 ⁴International Centre for Theoretical Physics (ICTP), Trieste, Italy

12
13 *Correspondence to:* Arona DIEDHIOU (arona.diedhiou@ird.fr)

14
15 **Abstract.** The latest version of RegCM4 with CLM4.5 as land surface scheme was used to
16 assess the performance and the sensitivity of the simulated West African climate system to
17 different convection schemes. The sensitivity studies were performed over the West Africa
18 domain from November 2002 to December 2004, at spatial resolution of 50km x 50km and
19 involved five (5) convective schemes: (i) Emanuel; (ii) Grell; (iii) Emanuel over land and
20 Grell over ocean (Mix1); (iv) Grell over land and Emanuel over ocean (Mix2); and (v)
21 Tiedtke. All simulations were forced with ERA-Interim data. Validation of surface
22 temperature at 2m and precipitation were conducted using respectively data from the Climate
23 Research Unit (CRU), Global Precipitation Climatology Project (GPCP) and Tropical
24 Rainfall Measurement Mission (TRMM) during June to September (rainy season), while the
25 simulated atmospheric dynamic was compared to ERA-Interim data. It is worth noting that
26 the few previous similar sensitivity studies conducted in the region was performed using
27 BATS as land surface scheme and involved less convective schemes. Compared with the
28 previous version of RegCM, RegCM4-CLM also shows a general cold bias over West Africa
29 whatever the convective scheme used. This cold bias is more reduced when using Emanuel
30 convective scheme. In term of precipitation, the dominant feature in model simulations is a
31 dry bias, better reduced when using Emanuel convective scheme. Considering the good
32 performance with respect to a quantitative evaluation of the temperature and precipitation
33 simulations over the entire West Africa domain and its sub-regions, Emanuel convective
34 scheme is recommended for the study of the West African climate system.

36

37 **1 Introduction**

38 Agriculture over West Africa relies mainly on rainfall and is strongly dependent on the West
39 African monsoon. Therefore, the onset, cessation and the amount of expected precipitation
40 associated with the West African Monsoon are of great importance for farmers and accurate
41 simulation and prediction of rainfall and temperature are crucial for various sectors, such as
42 agriculture, energy and health, and for decision-makers. Rainfall over West Africa is strongly
43 related to the meridional migration of the Inter-Tropical zone of convergence (ITCZ) and is
44 modulated by successive active and inactive phases of the monsoon system (Sultan et al.,
45 2003a; Janicot et al., 2011). After a quasi-stationary position around 5° N between mid-April
46 and end of June, the rainfall maxima present an abrupt shift toward the north to hold another
47 quasi-stationary position around 11°N in July-August, bringing precipitation over Central
48 Sahel region (Sultan and Janicot, 2000). This abrupt northward shift is the monsoon “onset”
49 over the Sahel and contrasts with the smooth southward retreat of the ITCZ, followed by the
50 second rainy season over the Guinean Coast in October–November (Sultan et al., 2003b;
51 Janicot et al., 2011). In addition, atmospheric circulations through African Easterly Jet (AEJ),
52 Tropical Easterly Jet (TEJ) and their interaction with convection play an important role in the
53 West African Monsoon (WAM) system (Nicholson 2013) and modulate the summer rainfall
54 (Sylla et al., 2013a). Various climate modeling tools have been applied over West Africa for
55 studying and better understanding of the WAM.

56 General circulation models (GCMs) are unable to include the effects of regional features (Xue
57 et al., 2010) due to their relatively coarse resolution. Regional Climate Models (RCMs) are
58 relevant tools for this purpose since they allow land surface heterogeneity and fine-scale
59 forcing such as complex topography and vegetation variations (Paeth and al., 2006).
60 Moreover, previous studies have shown that they are able to reasonably simulate the WAM
61 climatology (Kamga and Buscarlet, 2006; Sylla et al., 2009) and its variability (Diallo et al.,
62 2012). RCMs contributed to improve our knowledge of the interactions between atmospheric
63 and surface factors affecting the precipitation (Sylla et al., 2011; Browne and Sylla, 2012), of
64 the influence of external forcing such as Sea Surface Temperature (SST, Paeth and A. Hense,
65 2004), dust (Konare et al., 2008; N'Datchoh et al., 2017) and land-use changes on the dynamic
66 of the monsoon system (Abiodun et al., 2012; Zaroug et al., 2012).

67 RegCM versions (Giorgi et al., 2012; Pal et al., 2007) are the one of the most commonly used
68 among the large range of RCMs to study the climate of West African and of many regions of
69 the world. Compared with the previous version (RegCM3; Pal et al., 2007), the latest release

70 (RegCM4) has been improved with substantial development of the software code and of the
71 physical representations (Giorgi et al., 2012) and with the introduction of CLM (version 3.5
72 and 4.5) as an option to describe land surface processes. Previously it was Biosphere-
73 Atmosphere Transfer Scheme (BATS; Dickinson et al., 1993) only which was used as land
74 surface model. Many studies have shown that the model performs well when using BATS
75 over the West Africa (Sylla et al., 2009; Diallo et al., 2013) but CLM offers improvements in
76 the land-atmosphere exchanges of moisture and energy and in the associated surface climate
77 feedbacks (Steiner et al., 2009). Nonetheless it was shown over India that CLM use may lead
78 to a weaker performance of RegCM than BATS (Halder and al. (2015). Thus, the performance
79 of RegCM4 when using CLM (RegCM4-CLM4.5) needs to be assessed and sensitivities tests
80 have to be conducted on physical processes parameterization to find the optimal configuration
81 of the RCM for a given region and to give the relevant information to RCM users.

82 Among different physical processes in climate models, the convective parameterization is
83 usually considered as the most important when simulating the monsoon rainfall (Im et al.,
84 2008; Leung et al., 2004). Simulations of regional climate are very sensitive to physical
85 parameterization schemes, particularly over the tropics where convection plays a major role in
86 monsoon dynamics (Singh et al., 2011; Srinivas et al., 2013; Gao et al., 2016). One of the
87 main sources of uncertainties in climate prediction is related to the representation of the
88 clouds, which mainly influences the energy response of the models to a disturbance (Soden
89 and Held, 2006; IPCC, 2007). Thus, implementing appropriate convective scheme in dynamic
90 models is needed for realistic simulations.

91 Several sensitivity studies using previous version of RegCM have been conducted over
92 Africa. Meinke et al. (2007) and Djiotang and Kamga (2010) showed that in West Africa, the
93 monsoon precipitations are sensitive to the choice of cumulus parameterization and closure
94 schemes. Brown and Sylla (2012) performed a sensitivity study of RegCM3 to the domain
95 size over West Africa and showed that a large domain is required to capture variability of
96 summer monsoon rainfall and circulation features. Recent study by Adeniyi (2014) using
97 version 4 of RegCM indicated that all convective schemes give good spatial representation of
98 rainfall with biases over West Africa. Komkoua and al. (2016) found that the last release of
99 RegCM implementing Grell as convective scheme with Arakawa-Schubert closure
100 assumption is more suitable to downscale the diurnal cycle of rainfall over Central Africa.
101 However, none of these studies have attempted to investigate a sensitivity study of the
102 Regional Climate Model (RegCM4) to the convective scheme over West Africa with CLM4.5
103 as the land surface model.

104 This study investigates the performance of RegCM4-CLM4.5 over West Africa using
105 different convection schemes in the aim to identify the “best” configuration option for the
106 region. It is worth noting that the few previous similar sensitivity studies conducted in the
107 region was performed using BATS as land surface scheme and involved less convective
108 schemes. The paper is structured as follows: the description of the model, data and numerical
109 experiments used to investigate the RegCM4 performance are described in Section 2; Section
110 3 analyzes and discusses the model’s performance under different convection processes; and
111 the main conclusions are summarized in Section 4.

112

113 **2 Model description, observation datasets and numerical experiments**

114 **2.1 Model description and datasets.**

115 The 4th generation of the ICTP RegCM (hereafter RegCM4) is used in this study. RegCM is a
116 limited-area model using a terrain-following σ -pressure vertical coordinate system and an
117 Arakawa B-grid finite differencing algorithm (Giorgi et al., 2012). The model’s dynamical
118 component is derived from the hydrostatic version of the Pennsylvania State University
119 Mesoscale Model version 5 (MM5; Grell et al., 1994) with improvements on the coupling
120 with an advanced and complex land surface model (CLM3.5 and CLM4.5; Oleson et al., 2008
121 and 2013). In the version used here, the radiation scheme is derived from the NCAR global
122 model CCM3 (Kiehl et al., 1996) and includes representation of aerosols following Solmon et
123 al. (2006) and Zakey et al. (2006). Turbulent transports of momentum, water vapor and
124 sensible heat in the planetary boundary layer over land and ocean are computed as Holtslag et
125 al. (1990), which allows nonlocal transport in the convective boundary layer. The large-scale
126 precipitation scheme of Pal et al. (2000) referred as SUBgrid EXplicit moisture scheme
127 (SUBEX) includes the subgrid variability in clouds (Sundqvist and al., 1989) and the
128 evaporation and accretion processes for stable precipitation. Ocean surfaces fluxes of
129 momentum, heat and moisture are represented using the scheme of Zeng and al. (1998) with a
130 drag coefficient-based bulk aerodynamic procedure and considering the influence of surface
131 friction velocity on roughness length computed following Smith (1988) and Brutsaert (1982),
132 respectively for momentum and heat (and also moisture).

133 The soil-vegetation-atmosphere interaction processes are parameterized using Community
134 Land Model (CLM version 4.5; Oleson et al., 2013). CLM4.5 presents in each grid cell the
135 possibility to have fifteen soil layers, up to five snow layers, five different land unit types and
136 sixteen different plant functional types (Lawrence et al., 2011; Wang et al., 2016). RegCM4-
137 CLM4.5 proposes five different convective schemes (Im et al., 2008; Giorgi et al., 2012): the

138 modified-Kuo scheme (Anthes et al., 1987), the Tiedtke scheme (Tiedtke, 1989), the Emanuel
139 scheme (Emanuel, 1991), the Grell scheme (Grell, 1993) and the Kain-Fritsch scheme (Kain-
140 Fritsch, 1990; Kain, 2004) with the possibility to combine different schemes over ocean and
141 land (called as ‘mixed’ convection).

142

143 **2.2 Convective schemes**

144 The convective precipitation parameterizations used in this study are Tiedtke (1989), Emanuel
145 (1991) and Grell (1993) schemes.

146 The Emanuel (1991) scheme assumes that the mixing in clouds is highly episodic and
147 inhomogeneous (in contrary to a continuous entraining plume) and takes into account
148 convective fluxes based on an idealized model of sub-cloud-scale updrafts and downdrafts.
149 Convection is triggered when the level of neutral buoyancy is greater than the cloud base
150 level. Between these two levels, air is lifted and a fraction of the condensed moisture forms
151 precipitation while the remaining fraction forms the cloud. The cloud is supposed to mix with
152 the air from the environment according to a uniform spectrum of mixtures that ascend or
153 descend to their respective levels of neutral buoyancy. The mixing entrainment and
154 detrainment rates depend on the vertical gradients of buoyancy in clouds. Emanuel scheme
155 includes a formulation of the auto-conversion of cloud water into precipitation inside cumulus
156 clouds.

157 In the Grell (1993) scheme, deep convective clouds are represented by an updraft and a
158 downdraft that are undiluted and mix with environmental air only in cloud base and top.
159 Heating and moistening profiles are derived from latent heat released or absorbed, linked with
160 the updraft-downdraft fluxes and compensating motion (Martinez-Castro et al., 2006). Two
161 types of Grell scheme convective closure assumption can be found in RegCM4. In the
162 Arakawa–Schubert (1974) closure (AS), a quasi-equilibrium condition is assumed between
163 the generation of instability by grid-scale processes and the dissipation of instability by sub-
164 grid (convective) processes. In the Fritsch–Chappell (FC) closure (Fritsch and Chappell,
165 1980), the available buoyant energy is dissipated during a specified convective time period
166 (between 30 min and 1 hour).

167 Similarly, the Tiedtke (1989) scheme is a mass flux convection scheme, albeit it considers a
168 number of cloud types as well as cumulus downdrafts that can represent deep, mid-level and
169 shallow convection (Singh et al., 2011; Bhatla et al., 2016). The closure assumptions for the
170 deep and mid-level convection are maintained by large-scale moisture convergence, while the
171 shallow convection is sustained by the supply of moisture derived from surface evaporation.

172

173 **2.3 Numerical experiments and methodology**

174 Five experiments using the convection schemes of (1) Emanuel over land and Grell over
175 ocean (mix1), (2) Emanuel, (3) Grell, (4) Tiedtke and (5) Grell over land and Emanuel over
176 ocean (mix2) are conducted using RegCM4-CLM4.5 with 18 sigma levels at 50 Km
177 horizontal resolution for the period from November 2002 to September 2004. The two first
178 months (i.e. November and December 2002) was considered as spin-up time and not included
179 in the analysis. The years 2003 and 2004 has been selected in this study because they
180 corresponded respectively to dry and wet year in this region. The analyses will focus on the
181 rainy season from June to September (JJAS). As quantitative measurements of model skills,
182 we consider mean bias (MB) which is the difference between the area-averaged value of the
183 simulation and the observation, the spatial root mean square difference (RMSD) and the
184 spatial correlation called Pattern Correlation Coefficient (PCC) and the distribution of
185 Probability Density Function (PDF) of the temperature bias. The RMSD, PCC and the PDF
186 provide information at the grid-point level while the MB does so at the regional level. A
187 Taylor diagram (Taylor, 2001) is used to summarize assessments above and to show the
188 deviation of different model configurations results from observations.

189 As assumed in Gao et al. (2016), the temperature bias in JJAS present a normal mode type of
190 distribution. The PDF is expressed as:

$$191 \frac{1}{\sigma\sqrt{2\pi}} e^{-\frac{(x-\mu)^2}{2\sigma^2}}(1),$$

192 where μ is the mean and σ the standard deviation of temperature bias.

193 The PDF is characterized by its bell shaped curve, the temperature biases distribute
194 symmetrically around the mean bias temperature value in decreasing numbers as one moves
195 away from the mean. The empirical rule states that for a normal distribution, nearly all of the
196 data will fall within three standard deviations of the mean. The empirical rule can be broken
197 down into three parts:

- 198 • 68% of grid points fall within the first standard deviation from the mean.
- 199 • 95% of grid points fall within two standard deviations from the mean.
- 200 • 99.7% of grid points fall within three standard deviations from the mean.

201 The rule is also called the 68-95-99.7 Rule or the Three Sigma Rule. Thus, they constitute
202 measurements of model performance and systematic model errors. These metrics are
203 computed for each of the sub-regions indicated in Figure 1.

204 For this sensitivity study, the model was run at its standard configuration with 18 vertical
205 sigma layers (model top at 50 hPa) and with initial and boundary conditions provided by the
206 European Centre for Medium Range Weather Forecasts reanalysis ERA-interim (Simmons et
207 al., 2007; Uppala et al., 2008) at an horizontal resolution of 50 km and a temporal resolution
208 of 6 hours (00:00, 06:00, 12:00 and 18:00 UTC). Sea-surface temperatures (SST) were from
209 NOAA optimal interpolation weekly SST data (Reynolds et al., 2007). The terrain
210 characteristics (topography and land use data) were derived from United States Geological
211 Survey (USGS) and Global Land Cover Characterization (GLCC; Loveland et al., 2000)
212 respectively at 10 min horizontal resolution.

213 We focus our analysis on the precipitation and on the air temperature at 2m in the summer of
214 June-July-August-September (JJAS) over mainland West Africa. To reduce uncertainty due to
215 lack of surface climate observations over the region (Nikulin et al., 2012; Sylla et al., 2013a),
216 the simulated precipitation is validated using two observational datasets : the GPCP product
217 ($1^\circ \times 1^\circ$ resolution) is a satellite-derived dataset developed under the Global Precipitation
218 Climatology Project and made available from late 1996 to present and the 0.25° high
219 resolution dataset of Tropical Rainfall Measuring Mission 3B43V7 (TRMM) available from
220 1998 to 2013 (Huffman et al. 2007). The simulated 2m temperature is validated using also two
221 observational datasets including the Climate Research Unit (CRU) time series version 3.20
222 gridded at 0.5° horizontal resolution from the University of East Anglia and available
223 respectively from 1901 to 2011 (Harris et al., 2013), and the University of Delaware version
224 3.01 (UDEL) gridded dataset at 0.5° horizontal resolution available from 1900 to 2010
225 (Legates and Willmott, 1990). The simulated atmospheric fields are compared with ERA-
226 Interim reanalysis available from 1979 to present at 1.5° horizontal resolution (Dee et al.,
227 2011). All products have been regridded to $0.44^\circ \times 0.44^\circ$ using a bilinear interpolation method
228 to facilitate the comparison with RegCM4 simulations (Nikulin et al., 2012). The model's
229 performance is further examined in four sub-regions (Fig. 1), each with different
230 characteristics of the annual cycle of rainfall: Central Sahel ($10^\circ\text{W}-10^\circ\text{E}$; $10^\circ\text{N}-16^\circ\text{N}$), West
231 Sahel ($18^\circ\text{W}-10^\circ\text{W}$; $10^\circ\text{N}-16^\circ\text{N}$), Guinea Coast ($15^\circ\text{W}-10^\circ\text{E}$; $3^\circ\text{N}-10^\circ\text{N}$) and West Africa
232 ($20^\circ\text{W}-20^\circ\text{E}$; $5^\circ\text{S}-21^\circ\text{N}$).

233

234 **3 Results and discussion**

235 **3.1 Temperature**

236 The spatial distribution of averaged temperature during JJAS over 2003-2004 from CRU and
237 UDEL observations (resp. Fig. 2a, b) is compared to the temperature simulated by RegCM4

238 using the convection schemes: Mix1, Emanuel, Grell, Tiedtke and Mix2 (resp. Fig. 2c-g).
239 Figure 3 shows the associated mean model biases with areas statically significant at 95% of
240 confidence level (The dotted area denotes differences which are statistically significant at a
241 significance level of 0.05) relatively to CRU for observation (UDEL; Fig.3a) and the model
242 simulations (Fig. 3b-f). Table 1 reports the PCC and the RMSD between the simulated and
243 observed temperature calculated for Guinea Coast, Central Sahel, West Sahel and the entire
244 West Africa domain.

245 The CRU temperatures presents a zonal distribution in West Africa with maximum ($>34^{\circ}\text{C}$)
246 in the Sahara and lowest temperatures ($< 22^{\circ}\text{C}$) over the Guinea Coast and over complex
247 terrains such as the Jos plateau, Cameroon mountains and Guinean highlands. The Figure 3
248 show that the spatial distribution of the temperature biases is statically significance at 0.05
249 levels over most of the domain study. Except over the Guinea coast region and Cameron
250 Mountains. The UDEL observation (Fig. 2b) shows similarity with CRU in terms of spatial
251 distribution with PCC larger than 0.98 over the entire West African domain (see Table 1).
252 However, UDEL depicts a sparse distribution with a mixture of warm and cold bias over the
253 Sahara and along of Nigeria/Cameroon border around $\pm 2^{\circ}\text{C}$ (see Fig. 3a). There is also a good
254 agreement between model simulated temperatures and CRU observation with the PCCs more
255 than 0.93 (Table 1) over West Africa. All model configurations well reproduce the general
256 features of the observed pattern including the meridional surface temperature gradient zone
257 between Guinea Coast and the Saharan desert. This temperature gradient is important for the
258 evolution of the African Easterly Jet (AEJ) (Cook 1999; Thorncroft and Blackburn, 1999). All
259 model configurations (Fig. 3b-d, f) exhibit a similar dominant cold biases except the Tiedtke
260 configuration (Fig. 3e) in the Sahara desert at the central part of Mauritania and Niger, and
261 along the Guinea Coast region. The greater cold bias with value up to -5°C occurs when using
262 Grell configuration while, simulation using Tiedtke configuration depicts a dominant warm
263 bias up to 4°C mainly located in Central Sahel around 12°N (Fig. 3e). One effect of the warm
264 bias shown in Tiedtke simulation is to shift the zone of meridional temperature gradient
265 southward relative to its observed position (Fig. 2f). However, it is difficult to determine the
266 origin of RCM temperature biases as they involve changes in surface-atmosphere interactions
267 and as they are function of many factors such as surface albedo, cloudiness, temperature
268 advection and surface water and energy fluxes (Tadross et al., 2006; Sylla et al., 2012).

269 For a quantitative evaluation of the performance of these sensitivity tests, the PDF statistical
270 tool was used. The PDF distributions of the temperature bias in JJAS is shown in Figure 4 for
271 Guinea Coast, Central Sahel, West Sahel and the entire West Africa domain. The PDF

272 distribution shows a general dominant cold bias (see Fig. 4a-d) in model simulations over
273 most of study domain, except with Tiedtke configuration in the Central Sahel region.
274 Over Guinea Coast region, Grell configuration presents a colder bias with the maximum of
275 temperature bias distribution centered around -2°C (see Fig. 4a) compared to the other
276 configurations. However, Emanuel simulation shows the lower RMSD about 1.29°C with a
277 PCC larger than 0.77 (see Table 1). For Central Sahel region (Fig. 4b) a warmer bias is found
278 in Tiedtke simulation, while a colder bias is found in Grell and Mix2 configurations (see Fig.
279 4b). Emanuel configuration shows a lower value of RMSD about 0.67°C and a higher PCC
280 larger than 0.95 compared to the other model simulated temperatures (see table 1). In West
281 Sahel a colder bias is found with Grell scheme (see Fig. 4c) while Emmanuel and Tiedtke
282 simulations show a mixture of cold and warm bias. Configuration of RegCM with Emanuel
283 presents a better performance with a lower RMSD and higher PCC values compared to the
284 other simulations in West Sahel. Over the entire West Africa domain (see Fig.4d), Grell and
285 Tiedtke present respectively a colder and warmer bias. Generally, with respect to temperature
286 simulations, a better performance of RegCM4 is obtained when using Emmanuel scheme.

287

288 **3.2 Precipitation**

289 The spatial distribution of mean JJAS precipitation (2003–2004) over West Africa is shown in
290 Figure 5 for observations GPCP and TRMM (resp. Fig. 5 a-b) and for RegCM4 simulations
291 with the following convective schemes Mix1, Emmanuel, Grell, Tiedtke and Mix2 (resp.
292 Fig.5 c-g). Sylla et al. (2013a) argued that over Africa, GPCP is more consistent with gauge
293 based observations, whilst Nikulin et al. (2012) found a significant dry bias over tropical
294 Africa in TRMM compared to GPCP. We therefore select, for precipitation, GPCP as our
295 main observational reference in this paper. Figure 6 shows the corresponding precipitation
296 mean biases with statically significant at 95% of confidence level (The dotted area denotes
297 differences which are statistically significant at a significance level of 0.05) relatively to
298 GPCP for TRMM (Fig 6a) and for the different simulations configurations (Mix1, Emmanuel,
299 Grell, Tiedtke and Mix2; Fig 6b-f respectively). GPCP depicts a zonal band of rainfall
300 decreasing from North to South (see Fig. 5a). Precipitation maxima are found in orographic
301 regions of Guinea highlands, Jos Plateau, and Cameroon Mountains. The Figure 6 show that
302 the spatial distribution of the precipitation biases is statically significance at 0.05 levels over
303 almost the domain study. Differences between TRMM and GPCP observation products (Table
304 2) can reach up to -5.26% at sub-regional levels, while over the entire West Africa it does not
305 exceed 0.82% . Although both observation products exhibit some differences (Fig.6a), their

306 patterns show a good agreement, with PCCs more than 0.96 over the entire West Africa
307 domain (Table 2). TRMM underestimates the rainfall intensity over Guinea Coast and Central
308 Sahel regions (respectively no more than -0.86% and -5.12%) and overestimates the rainfall
309 intensity over West Sahel and the entire West Africa domain reaching respectively 3.48% and
310 0.83%. The spatial distribution of rainfall is well reproduced by all model configurations with
311 PCCs values within the range 0.61 and 0.89 over the entire West African domain. The
312 dominant feature in these simulations is the dry bias over West Africa domain (Fig. 6b-f),
313 which is more pronounced in the Tiedtke configuration (see Table 2). The warmer bias over
314 Central Sahel in Tiedtke configuration (Fig.3e) is consistent with the drier bias found in the
315 same region (see Table 2 and Fig.6e), as less rainfall would induce less evaporative cooling
316 (decrease of latent heat flux) and therefore less favorable conditions for cloud cover (Feddem
317 et al. 2005). The decrease of the cloud cover will lead to an increase of incident radiation
318 inducing an increase of sensible heat flux and warmer surface temperatures. Moreover, a drier
319 bias may be associated with a heating induced by the adiabatic subsidence to compensate
320 effect of the increase of the surface albedo (Charney 1975). However, the Table 2 reveals that
321 Mix1 and Emanuel show a better performance with a lower mean biases and greater PCC
322 compared to the others model simulations over the entire West African domain and its sub-
323 regions.

324 In order to understand the origins of the model rainfall biases, we analyzed the JJAS midlevel
325 (850–300 hPa) vertically integrated water vapor mixing ratio and the 650 hPa low-level wind
326 (African Easterly jet, AEJ) over West Africa averaged over the 2003–2004 period (Fig. 7).
327 The AEJ is the most prominent feature affecting the West African Monsoon through its role
328 in organizing convection and precipitation over the region (Cook, 1999; Diedhiou et al., 1999;
329 Mohr and Thorncroft, 2006; Sylla et al., 2011). Areas with larger water vapor mixing ratio
330 corresponds to the areas of maximum precipitation in observations (see Fig. 5a-b). Around
331 9°N the weaker easterly wind (AEJ) contributes to enhance the moisture convergence which
332 results in an increase of water vapor and precipitation (see Fig. 5a-b). All model
333 configurations show some quantitative differences compared to ERA-Interim in both the wind
334 flux and the water vapor mixing ratio.

335 The underestimation of vertically integrated water vapor mixing ratio is larger in Grell and
336 Mix2 simulations (Fig. 7 c, e) over the Guinea Coast and Atlantic Ocean compared to those of
337 Mix1, Emanuel and Tiedtke (Fig. 7 a, b, e). Mix1 and Emanuel configurations reproduce
338 better the spatial extent of the moisture convergence than the others model configurations
339 (Fig.7b, c). All model configurations simulate a stronger easterly wind flux (AEJ) than

340 observed in particular over the Guinea Coast and Atlantic Ocean inducing a negative impact
341 on simulated precipitations in the sub-regions (see Fig. 5c–g). Another possible explanation
342 of model rainfall biases is further discussed in Brown and Sylla (2011) whereby a sensitivity
343 study on the domain size with RegCM3 over West Africa showed that RegCM3 simulates
344 drier conditions over a default domain (RegCM-D1) quite similar to our domain size used in
345 this study.

346 A Taylor diagram is used to give a combined synthesized view of the pattern correlation
347 coefficient and the JJAS standard deviation of precipitation from the different sensitivity
348 studies with respect to GPCP over Guinea Coast, Central Sahel, West Sahel and West Africa.
349 Model standard deviations are normalized by the observed value from GPCP (indicated by
350 REF, see Fig.8). For the entire West Africa domain, the diagram shows Tiedtke and Emanuel
351 outperform the others configurations with values of standard deviation normalized much
352 closer to 1. However Emanuel configuration present a better spatial correlation reaching 0.8
353 as compared to Tiedtke configuration. Over Guinea Coast sub-region Grell and Emanuel
354 present better values of standard deviation normalized. However, in regarding the spatial
355 correlation value about 0.7 Emanuel configuration is the best. For West and Central Sahel,
356 Mix1 and Emanuel are closer to observation. However, Emanuel outperforms Mix1
357 configuration with a good spatial correlations scores between 0.7 and 0.8 respectively over
358 Central and West Sahel sub-regions. From the Taylor diagram, it can be inferred that Emanuel
359 performs better regarding the standard deviation normalized and the pattern correlation over
360 the entire West African domain and its sub-regions.

361 Based on previous experience and studies, Gao and al. (2016) noted that use of the Emanuel
362 convection scheme in RegCM3 and RegCM4 over China tends to simulate too much
363 precipitation when using BATS as the land surface scheme. They explained that it is mainly
364 due to the fact that the Emanuel scheme responds quite strongly to heating from the surface
365 land as compared to Grell and Tiedtke convection schemes, once convection is triggered.
366 BATS with only two soils levels depth maximizes this response; this is why Emmanuel is too
367 wet when using BATS as compared to Grell and Tiedtke. By contrast, CLM uses several soil
368 layers down to a depth of several meters; therefore, the upper soil temperatures respond less
369 strongly to the solar heating. Precipitation amount is much reduced when using CLM, which
370 is good for Emanuel but not good for Grell and Tiedtke (Gao and al., 2016) while the
371 combination of BATS with Grell and Tiedtke shows good performance (Gao et al., 2012; Ali
372 et al., 2015).

373 In conclusion, although RegCM4-CLM4.5 shows some weaknesses, such as a dry bias over
374 most of Central Sahel and Guinea Coast region, its performance in replicating the spatial
375 distribution of rainfall appears in line with that documented in previous studies using the
376 previous version RegCM3 (Sylla et al., 2009; Abiodun et al., 2012).

377

378 **3.3 Mean annual cycle**

379 In this section, we examine the effect of the convection scheme in the characterization of the
380 three distinct phases of the West African Monsoon: the onset, the high rain period and the
381 southward retreat of the monsoon rain band (Sultan et al., 2003). Such behavior is best
382 represented by a meridional cross-section (time-latitude Hovmoller diagram). This diagram
383 provides a robust framework to assess RCM's skills in simulating seasonal and intraseasonal
384 variations of the WAM, and thus the mechanisms of the region's rainfall (Hourdin et al.,
385 2010). Figure 9 shows the time-latitude diagrams of rainfall averaged over the region between
386 10°E and 10°W for observations GPCP and TRMM (resp. Fig 9a-b) and for model
387 simulations using Mix1, Emmanuel, Grell, Tiedtke and Mix2 convection schemes (resp. Fig
388 9c-g). The averages are taken for the period 2003–2004 and displayed throughout the year.
389 This figure shows that the cores of the different phases are well marked in TRMM than in
390 GPCP (resp. Fig.9a, b). TRMM observation shows a first rainy season from mid-March up to
391 mid-June over the Gulf of Guinea and Guinea Coast with a northward extension of the rain
392 belt up to about 5°N (Fig.9b). The monsoon jump is characterized by a sudden cessation of
393 precipitation intensities (Sultan and Janicot, 2000, 2003) and occurs from mid-June to early
394 July, when the rain band core moves suddenly northward to about 10°N (Fig.9b). This
395 indicates the beginning of the rainy season over the Sahel with a peak reached in August
396 between 9° and 12°N over Central Sahel. A gradual retreat of the monsoon starts in end of
397 August and it is well shown by GPCP (Fig.9a), with a decrease in intensity and a southward
398 migration of the rain band. There are both similarities and differences across the two
399 observation datasets TRMM and GPCP. Both datasets agree in area of rainfall maximum
400 intensity around 4°N despite a more intense peak of rainfall for TRMM compare to GPCP
401 (resp. Fig.9a, b). The monsoon jump characterized by a discontinuity sharp is not well defined
402 in GPCP compared to TRMM. In addition, GPCP shows wet conditions during the retreat
403 phase in July to September compared to TRMM (Fig.9a, b).

404 Mix1, Emanuel, and Grell model configurations (resp. Fig.9c-e) capture the three phases of
405 the seasonal evolution of the WAM, while Tiedtke and Mix2 simulations fail to reproduce
406 them in particular the rainy season over Central Sahel. However Emanuel and Mix model

407 configurations (resp. Fig. 6c, d) overestimate rainfall amounts during the two rainy seasons
408 over Guinea Coast, mostly as a result of an overestimate of the precipitation over the
409 orographic regions of Guinea highlands, Jos Plateau, and Cameroon Mountains. Mix1 and
410 Mix2 configurations are respectively wetter and drier compared to the others model
411 configurations (resp. Fig. 9c, g). Generally, the three monsoon phases are well shown by Grell
412 simulation, albeit it is drier compared to the others model simulations.

413 Another analysis of the annual cycle consists of considering the area-averaged (land-only grid
414 points) value of monthly rainfall and temperature over the Gulf of Guinea, the Central Sahel
415 and the entire West African domain (Figures 10 and 11). This allows better identification of
416 rainfall and temperature minima and peaks. Figure 10a-d shows respectively the annual cycle
417 of precipitation averaged over Guinea Coast, Central Sahel, West Sahel and the entire West
418 African domain. Over the Guinea Coast (Fig 10a), both GPCP and TRMM observations show
419 a primary maximum in June and a secondary one in September. The Mix1 and Tiedtke model
420 configurations simulate an early first peak in May while Emanuel, Grell and Mix2
421 configurations well capture the observed peak in June. We note that model configurations
422 well reproduce the timing of the mid-summer break and second rainfall peak in September but
423 they underestimate its magnitude, although Mix1 simulation result is higher and much closer
424 to observations compared to the others model simulations.

425 In both Central Sahel and West Sahel, observations (GPCP and TRMM) display a dry spring
426 (from January to March) and winter (from October to December) and a wet summer (from
427 June to September) with a well-defined peak occurring in August. Model configurations
428 reproduce both phase of the annual cycle and the observed rainfall peak in August except
429 Emanuel configuration which shifts it in September over West Sahel region. Model
430 simulations underestimate the peak intensity compare to observations. However Mix1
431 configuration rainfall peak is much closer to observation for both Central Sahel and West
432 Sahel regions (resp. Fig 10b, d) compared to the others model simulations. Over the entire
433 West African domain, the annual cycle (Fig 10c) is smoother with a notable shift of the peak
434 in September in the different model configurations. All the model configurations
435 underestimate the rainfall peak and shift it in October. However, Mix1 and Emanuel model
436 simulations are much closer to observed annual cycle of precipitation compared to the others.
437 In resume Mix1 simulation compared to the others better reproduce the observed annual cycle
438 of precipitation over the sub-regions and the entire West African domain.

439 The annual cycles of temperature for Central Sahel, West Sahel and the entire West African
440 domain of Mix1, Emmanuel, Grell, Tiedtke and Mix2 convection schemes are shown in

441 Figure 11b-d. The observations (CRU and UDEL) indicate a cooler winter from December to
442 February and warmer pre and post-monsoon periods with relative minima occurring during
443 August. While over Guinea Coast, both winter and post monsoon are cooler and only the pre
444 monsoon phase is warmer (Fig. 11a). Models configurations present similar seasonal variation
445 of the mean monthly temperature at 2 m compared to observations, but do exhibit some
446 differences.

447 Over Guinea Coast model simulations underestimate the magnitude of the temperature
448 compared to observations. However, Tiedtke configuration is higher and much closer to
449 observations compared to the others model simulations throughout the year (Fig.11a). Over
450 Central Sahel region, Grell and Tiedtke capture well the seasonal variation from November to
451 June in particular the first peak in August compared to the others models simulations. During
452 the summer (JJAS) Emanuel and Mix1 quite well reproduce the observed precipitation annual
453 cycle (Fig.11b). Therefore, model simulations underestimate the seasonal variation of
454 temperature over the entire West African domain. Although Tiedtke simulation overestimates
455 the mid-summer break period, it is much closer to observed annual cycle of temperature
456 throughout the year compared to the others model simulations. Over the West Sahel, model
457 simulations quite well reproduce the annual cycle of temperature except Grell and Mix2
458 configurations in particular during the summer (JJAS). In summary Tiedtke simulation better
459 reproduce the observed annual cycle of temperature throughout the year over the sub-regions
460 and the entire West African domain compared to the others model configurations.

461 The divergences in the RCMs annual cycles arise mostly from their different abilities to
462 simulate the main features responsible of triggering and maintaining the WAM precipitation
463 (Gbobaniyi E. et al., 2013). Among them, we have the monsoon flow, the African Easterly Jet
464 (AEJ), the Tropical Easterly Jet (TEJ) and the Africa Easterly Waves (AEWs) (Diedhiou et
465 al., 1999; Sylla et al., 2013b). .

466

467 **3.4 Wind profile**

468 The atmospheric circulations and their interactions with ITCZ play an important role in the
469 WAM system (Nicholson, 2013). Thus, this section aims to analyze the impact of the choice
470 of convection scheme in the simulations of zonal winds features, including the near-surface
471 westerly component (the West African Monsoon, WAM), the African Easterly Jet (AEJ) and
472 the Tropical Easterly Jet (TEJ) in the mid and upper troposphere respectively. Figure 12
473 depicts the vertical cross section of the JJAS mean of the zonal wind averaged between 10°W
474 and 10°E for ERA-Interim (Fig.12a) and model configurations in Mix1, Emmanuel, Grell,

475 Tiedtke and Mix2 convection schemes (resp. Fig.12 b-f). The reanalyse ERA-Interim (Fig.
476 12a) displays the monsoon flow winds below 800 hPa at 2-18°N with two cores merged over
477 both Guinea Coast (centered at 6°N) and Central Sahel (centered at 15°N) sub-regions, the
478 AEJ in the mid-levels centered at 12°N and the TEJ in the upper tropospheric levels at 200
479 hPa centered at 5°N (Fig12 a). All model configurations well reproduce the zonal wind
480 features despite some biases.

481 Model simulations Mix1, Emanuel, Grell and Tiedtke present a strong core of monsoon flow
482 compared to Era-Interim (reaching 6m/s). The stronger and weaker monsoon flows are found
483 with Mix1 and Mix2 configurations respectively compared to the others configurations.
484 However, model simulations well reproduce the limit of the surface westerly flow compared
485 to its position. Of particular interest is the core of the AEJ in the mid-tropospheric levels,
486 which is greatly weakened with Mx1 and Emanuel. While AEJ magnitude core is well
487 defined in Grell and Mix2 simulations at 12°N, but its spatial extent is somewhat reduced.
488 This location of the AEJ in Grell and Mix2 simulation is consistent with the location of the
489 region of zonal temperature gradient (see resp. Fig. 3e, g), as the AEJ is associated with the
490 surface temperature gradient (Cook, 1999; Thorncroft and Blackburn, 1999). While Tiedtke
491 simulation shifts the location of AEJ core at 8°N in agreement with the warm bias shown in
492 Tiedtke configuration (see Fig.4e). The TEJ at 200 hPa and 5°N is very similar in model
493 simulations compared to the ERA-Interim reanalysis. However, the core of the jet is weaker
494 in Tiedtke configuration compared to the others model simulations. An overall, Grell
495 configuration outperforms simulations of the main features of the zonal wind compared to the
496 others model simulations.

497

498 **4 Summary and conclusion**

499 The latest released RegCM4 have been performed over West Africa for two years (2002-
500 2003) to assess its performance using five convective parameterizations: (a) the Emanuel
501 scheme, (b) Emanuel over land and Grell over Ocean (Mix1), (c) the Grell scheme, (d) the
502 Tiedtke scheme and (e) Grell over land and Emanuel over Ocean scheme (Mix2). The
503 sensitivity of the model to different convection schemes were validated using observations.
504 The main findings and conclusions can be summarized as follows:

- 505 (1) Compared with the previous version of RegCM, RegCM4-CLM also shows a general
506 cold bias over West Africa. However in Central Sahel region, Tiedtke simulation
507 presents a warm bias. This warm bias tends to displace the meridional temperature

508 gradient southward relative to its observed position. An overall, with respect to
509 temperature, better performance are obtained when using Emanuel scheme.

510 (2) With respect to the precipitation, the dominant feature in model simulations is a dry
511 bias which is more pronounced when using Tiedtke convection scheme. Considering
512 the good performance over the entire West Africa domain and its sub-regions in the
513 temperature and precipitation simulations, we suggest Emanuel convection scheme
514 when using RegCM4-CLM4.5 over West Africa.

515 (3) Simulations when using Mix1 and Emanuel schemes well reproduce the spatial extent
516 of moisture convergence of the ERA-Interim reanalyses compared to the others
517 convection schemes. However, in the mid-levels of the atmosphere, model simulations
518 show an easterly wind flux (AEJ) stronger than observed in particular over the Guinea
519 Coast and Ocean Atlantic below the latitude 4°N , creating an increased subsidence
520 and has a negative effect on simulated precipitations there. This is a possible
521 explanation of a dry bias over West Africa domain. However, the vertical features of
522 the zonal wind, including the near-surface westerly component, the AEJ and the TEJ
523 in the mid and upper troposphere are better simulated when using Grell convection
524 scheme compared to the others model simulations

525 (4) The time evolution of simulation when using Grell convection scheme rainfall
526 matches well with the observed evolution, including the timing of the discontinuous
527 northward jump of the main rainfall band in late June, albeit it is drier compared to
528 Mix1 and Emanuel convection scheme.

529 (5) Over Central Sahel and West Sahel, the mean annual cycle of precipitation and
530 temperature, with the single peaked rainy season is especially well captured in terms
531 of timing despite the fact that all model simulations underestimated the magnitude.
532 However, simulations using Mix1 reproduce better the annual cycle of precipitation
533 compared to the others schemes.

534 (6) Over Guinea Coast, Mix1 and Tiedtke model simulations failed to reproduce the
535 double peaks rainy seasons, while Emanuel, Grell and Mix2 simulations well
536 reproduce them but underestimate their amplitude. The bimodal nature of rainfall
537 associated with the Guinea sub-region is not so well defined when averaging rainfall
538 over the entire West African domain. This emphasizes the importance of separating
539 regions into homogeneous precipitation sub-regions for evaluation analyses.

540 (7) The mean annual cycle of temperature, is well reproduce in simulation when using
541 Tiedtke convection scheme throughout the year over the sub-regions and the entire
542 West Africa domain compared to the others model simulations.

543

544 As more advanced package compared to the previously version of RegCM with BATS,
545 CLM4.5 can be considered as the primary land surface processes option in RegCM4. Therein,
546 the use of Emanuel scheme is recommended over the West African region. We plan to use
547 this configuration in long-term, multi-decadal simulations, to further evaluate the model
548 capability in reproducing the mean climatology. To bring up this study more complete, we
549 will study the sensitivity of temperature and precipitation extremes simulated by RegCM4-
550 CLM4.5 to different convective schemes.

551

552 **Acknowledgements**

553 This work is dedicated to the memory of Prof Abdourahamane Konaré with whom we started
554 this assessment. The authors thank the Institute of Research for Development (IRD, France)
555 and Institute of Geosciences for Environment (IGE, University Grenoble Alpes) for providing
556 the facility (the Regional Climate Modelling Platform) to perform these simulations and the
557 IT support funded by IRD/PRPT contract at the University Felix Houphouet Boigny (Abidjan,
558 Côte d'Ivoire). The authors are grateful to all students, technicians, engineers and researchers
559 involved at ICTP (Abdus Salam International Centre of Theoretical Physics; Trieste, Italy) on
560 the development and the improvement of the regional climate model RegCM.

561

562 **References**

- 563 Abiodun BJ, Adeyewa ZD, Oguntunde PG, Salami AT, Ajayi VO. 2012. Modeling the
564 impacts of reforestation on future climate in
565 West Africa. *Theor. Appl. Climatol.* 110(1–2): 77–96.
566
- 567 Adeniyi MO. 2014. Sensitivity of different convective schemes in RegCM4.0 for simulation
568 of precipitation during the Septembers of 1989 to 1998 over West Africa. *Theor. Appl.*
569 *Climatol.* 115(1–2): 305–322, doi: 10.1007/s00704-013-0881-5.
570
- 571 Adler RF et al (2003). The version-2 Global Precipitation Climatology Project (GPCP)
572 monthly precipitation analysis (1979–present). *J Hydrometeorol* 4(6):1147–1167
573
- 574 Ali S., L. Dan, C. B. Fu, and Y. Yang, 2015: Performance of convective parameterization
575 schemes in Asia using RegCM: Simulations in three typical regions for the period 1998–2002.
576 *Adv. Atmos. Sci.*, 32(5), 715–730, doi:10.1007/s00376-014-4158-4.h
577
- 578 Arakawa A, Schubert WH (1974) Interaction of a cumulus cloud ensemble with the large
579 scale environment. Part I. *J Atmos Sci* 31: 674–701
580
- 581 Bhatla R., S. Ghosh, B. Mandal, R.K. Mall, Kuldeep Sharma. "Simulation of Indian summer
582 monsoon onset with different parameterization convection schemes of RegCM-4.3",
583 *Atmospheric Research*, 2016. DOI : 10.1016/j.atmosres.2016.02.010
584
- 585 Browne N.A.K., Sylla MB. 2012. Regional climate model sensitivity to domain size for the
586 simulation of the West African monsoon rainfall. *Int. J. Geophys.* Article ID 625831, DOI:
587 10.1155/2012/625831.
588
- 589 Brutsaert W (1982) *Evaporation into the atmosphere: theory, history and applications.* USA:
590 Reidel Hingham Mass, 299 pp
591
- 592 Charney, J. G. (1975). Dynamics of deserts and drought in the Sahel. *Quarterly Journal of the*
593 *Royal Meteorological Society*, 101(428), 193-202.

594 Cook, K. H., 1999: Generation of the African easterly jet and its role in determining West
595 African precipitation. *J. Climate*, 12, 1165–1184, doi:10.1175/1520-
596 0442(1999)012,1165:GOTAEJ.2.0.CO;2.

597

598 Dee et al (2011) The ERA-Interim reanalysis: configuration and performance of the data
599 assimilation system. *Quat J R Meteorol Soc* 137:553–597. doi:10.1002/qj.828

600

601 Diallo I, Sylla MB, Camara M, Gaye AT. 2012. Interannual variability of rainfall and
602 circulation features over the Sahel based on multiple regional climate models simulations.
603 *Theor. Appl. Climatol.* DOI:10.1007/s00704-012-0791-y.

604

605 Diallo I, Sylla MB, Camara M, Gaye AT (2013) Interannual variability of rainfall over the
606 Sahel based on multiple regional climate models simulations. *Theor Appl Climatol.*
607 doi:10.1007/s00704-012-0791-y

608

609 Dickinson, R., A. Henderson-Sellers, and P. Kennedy. 1993. “Biosphere-Atmosphere
610 Transfer Scheme (BATS) Version 1eas Coupled to the NCAR Community Climate Model.”
611 NCAR Technical Note, NCAR/TN-387+ STR, 72 pp.

612

613 Diedhiou, A., Janicot, S., Viltard, A., De Felice, P., & Laurent, H. (1999). Easterly wave
614 regimes and associated convection over West Africa and tropical Atlantic: Results from the
615 NCEP/NCAR and ECMWF reanalyses. *Climate Dynamics*, 15(11), 795-822.

616

617 Djiotang Tchotchou LA, Mkankam Kamga F. 2010. Sensitivity of the simulated African
618 monsoon of summers 1993 and 1999 to convective parameterization schemes in RegCM3.
619 *Theor. Appl. Climatol.* 100: 207–220.

620

621 Emanuel, K. 1991. “A Scheme for Representing Cumulus Convection in Large-Scale
622 Models.” *Journal of the Atmospheric Sciences* 48: 2313-2329.

623

624 Emanuel KA, Zivkovic-Rothman M (1999) Development and evaluation of a convection
625 scheme for use in climate models. *J Atmos Sci* 56:1766–1782

626

627 Feddema, J. J., Oleson, K. W., Bonan, G. B., Mearns, L. O., Buja, L. E., Meehl, G. A., &
628 Washington, W. M. (2005). The importance of land-cover change in simulating future
629 climates. *Science*, 310(5754), 1674-1678.

630

631 Fritsch JM, Chappell CF (1980) Numerical prediction of convectively driven mesoscale
632 pressure systems. Part I: Convective parameterization. *J Atmos Sci* 37: 722–1733

633

634 Gao, X., Y. Shi, D. Zhang, J. Wu, F. Giorgi, Z. Ji, and Y. Wang. 2012. “Uncertainties in
635 Monsoon Precipitation Projections over China: Results from Two High-Resolution RCM
636 Simulations.” *Climate Research* 52: 213–226.

637

638 Gao Xue-Jie, Ying SHI, Filippo GIORGI, (2016). Comparison of convective
639 parameterizations in RegCM4 experiments over China with CLM as the land surface model.
640 *Atmospheric and Oceanic Science Letters*, 9:4, 246-254, DOI:
641 10.1080/16742834.2016.1172938

642

643 Gbobaniyi E, Sarr A, Sylla MB, Diallo I, Lennard C, Diedhiou A et al (2013) *Climatology,*
644 *annual cycle and interannual variability of precipitation and temperature in CORDEX*
645 *regional climate models simulation over West Africa. Inter J Climatol.* doi:10.1002/joc.3834

646

647 Giorgi F, Coppola E, Solmon F, Mariotti L, Sylla MB, Bi X, Elguindi N, Diro GT, Nair V,
648 Giuliani G, Cozzini S, Guettler I, O’Brien T, Tawfik A, Shalaby A, Zakey AS, Steiner A,
649 Stordal F, Sloan L, Brankovic C. 2012. RegCM4: model description and preliminary tests
650 over multiple CORDEX domains. *Climate Res.* 52: 7–29, DOI:v10.3354/cr01018.

651

652 Grell G, Dudhia J, Stauffer DR (1994) A description of the fifth generation Penn State/NCAR
653 Mesoscale Model (MM5). National Center for Atmospheric Research Tech Note NCAR/TN-
654 398+STR, NCAR, Boulder, CO

655

656 Grell, G. 1993. “Prognostic Evaluation of Assumptions Used by Cumulus Parameterizations.”
657 *Monthly Weather Review* 121: 764-787.

658

659 Halder S., Dirmeyer P. and K. Saha, 2015. “Sensitivity of the Mean and Variability of Indian
660 Summer Monsoon to Land Surface Schemes in RegCM4: Understanding Coupled Land-
661 Atmosphere Feedbacks.” *Journal of Geophysical Research* 120:9437–9458
662

663 Harris I, Jones PD, Osborn TJ, Lister DH (2013) Updated high-resolution grids of monthly
664 climatic observations. *Int J Climatol*. doi:10.1002/joc.3711
665

666 Holtslag A, De Bruijn E, Pan H-L (1990) A high resolution air mass transformation model for
667 short-range weather forecasting. *Mon Wea Rev* 118: 1561–1575
668

669 Huffman GJ, Adler RF, Bolvin DT, Gu G, Nelkin EJ, Bowman KP, Hong Y, Stocker EF,
670 Wolff DB (2007) The TRMM multisatellite precipitation analysis: quasi-global, multi-year,
671 combined-sensor precipitation estimates at fine scale. *J Hydrometeorol* 8:38–55
672

673 Hourdin F, Musat I, Guichard F, Ruti PM, Favot F, Filiberti MA, Pham M, Grandpeix JY,
674 Polcher J, Marquet P, Boone A, Lafore JP, Redelsperger JL, Dell’aquila A, Doval TL, Traore
675 AK, Gall’ee H. 2010. AMMA-model intercomparison project. *Bull. Am. Meteorol.Soc.* 91(1):
676 95–104.
677

678 Im, E., J. Ahn, A. Remedio, and W.-T. Kwon. 2008. “Sensitivity of the Regional Climate of
679 East/Southeast Asia to Convective Parameterizations in the RegCM3 Modelling System. Part
680 1: Focus on the Korean Peninsula.” *International Journal of Climatology* 28: 1861–1877.
681

682 IPCC. 2007. *Climate Change 2007: The Physical Science Basis*. Contribution of Working
683 group I to the Fourth Assessment Report of the Intergovernmental Panel on Climate Change,
684 Solomon S, Qin D, Manning M, Chen Z, Marquis M, Averyth KB, Tignor M, Miller HL (eds).
685 Cambridge University Press: Cambridge, UK, 996 pp.
686

687 Janicot S, Caniaux G, Chauvin F, de Coetlogon G, Fontaine B, Hall N, Killadis G, Lafore J-P,
688 Lavaysse C, Lavender SL, Leroux S, Marteau R, Mounier F, Philippon N, Roehrig R, Sultan
689 B, Taylor CM (2011) Intraseasonal variability of the West African monsoon. *Atmos Sci Lett*
690 12:58–66. doi:10.1002/asl.280
691

692 Kain, J. S., and J. M. Fritsch, 1990: A one-dimensional entraining/detraining plume model
693 and its application in convective parameterization. *J. Atmos. Sci.*, 47, 2784–2802.
694

695 Kain J. S, 2004. The Kain–Fritsch Convective Parameterization: An Update. *Journal of*
696 *Applied Meteorology*. Vol. 43, Issue 1, pp.170-181.
697

698 Kamga Foamouhoue A, Buscarlet ' E. 2006. Simulation du climat de l’Afrique de l’Ouest à
699 l’aide d’un modèle climatique régional: validation sur la période 1961–1990.
700

701 Komkoua Mbienda A. J., Tchawoua C., Vondou D. A., Choumbou P., Kenfack Sadem C.,
702 and Dey S, 2016. Sensitivity experiments of RegCM4 simulations to different convective
703 schemes over Central Africa. *Int. J. Climatol.* DOI: 10.1002/joc.4707
704

705 Kiehl JT Hack JJ, Bonan GB, Boville BA, Briegleb BP, Williamson DL, Rasch PJ (1996)
706 Description of the NCAR Community Climate Model (CCM3). Technical Note NCAR/TN—
707 420+STR, p 152
708

709 Konare A, Zakey AS, Solmon F, Giorgi F, Rauscher S, Ibrah S, Bi X. 2008. A regional
710 climate modeling study of the effect of desert dust on the West African monsoon. *J. Geophys.*
711 *Res.* 113(D12): D12206.
712

713 Meinke I, Roads J, Kanamitsu M. 2007. Evaluation of RSM-simulated precipitation during
714 CEOP. *J. Meteorol. Soc. Jpn.* 85A: 145–166.
715

716 Mohr, K. I., and C. D. Thorncroft, 2006: Intense convective systems in West Africa and their
717 relationship to the African easterly jet. *Quart. J. Roy. Meteor. Soc.*, 132, 163–176,
718 doi:10.1256/qj.05.55.
719

720 N'Datchoh E. T. , Diallo I., Konaré A., Silué S., Ogunjobi K.O., Diedhiou A., Doumbia M.
721 (2017) Dust induced changes on the West African summer monsoon features. *Int J Climatol*,
722 DOI: 10.1002/joc.5187.
723

724 Nicholson SE (2013) The West African Sahel: a review of recent studies on the rainfall
725 regime and its interannual variability. *Meteorology*. Volume 2013, Article ID 453521, 32
726 pages. doi:10.1155/2013/453521
727

728 Nikulin G, Jones C, Samuelsson P, Giorgi F, Asrar G, Bu'chner M, Cerezo-Mota R,
729 Christensen OB, De'que' M, Fernandez J, Hansler A, van Meijgaard E, Sylla MB, Sushama L
730 (2012) Precipitation climatology in an ensemble of CORDEX-Africa regional climate
731 simulations. *J Clim* 6057–6078. doi:10.1175/JCLI-D-11-00375.1
732

733 Lawrence, D. M., et al. (2011), Parameterization improvements and functional and structural
734 advances in version 4 of the Community Land Model, *J. Adv. Model. Earth Syst.*, 3, M03001,
735 doi:10.1029/2011MS000045.
736

737 Legates DR, Willmott CJ (1990) Mean seasonal and spatial variability in gauge-corrected,
738 global precipitation. *Int J Climatol.*, 10:111–127
739

740 Leung, L., S. Zhong, Y. Qian, and Y. Liu. 2004. "Evaluation of Regional Climate Simulations
741 of the 1998 and 1999 East Asian Summer Monsoon Using the GAME/HUBEX Observational
742

743 Loveland TR, Reed BC, Brown JF, Ohlen DO, Zhu J, Yang L, Merchant JW (2000)
744 Development of a global land cover characteristics database and IGBP DISCover from 1-km
745 AVHRR Data. *Int J Remote Sensing* 21: 1303–1330
746

747 Martinez-Castro, D., da Rocha, R. P., Bezanilla-Morlot, A., Alvarez-Escudero, L., Reyes-
748 Fernández, J. P., Silva-Vidal, Y., & Arritt, R. W. (2006). Sensitivity studies of the RegCM3
749 simulation of summer precipitation, temperature and local wind field in the Caribbean
750 Region. *Theoretical and Applied Climatology*, 86(1-4), 5-22. DOI 10.1007/s00704-005-0201-
751 9.
752

753 Oleson, K., G. Niu, Z. Yang, D. Lawrence, P. Thornton, P. Lawrence, et al., 2008.
754 "Improvements to the Community Land Model and Their Impact on the Hydrological Cycle."
755 *Journal of Geophysical Research* 113: G01021. doi: <http://dx.doi.org/10.1029/2007JG000563>.
756

757 Oleson KW, Lawrence DM, Bonan GB et al (2013) Technical description of version 4.5 of
758 the Community Land Model (CLM). NCAR technical note NCAR/TN-503 + STR. National
759 Center for Atmospheric Research, Boulder
760

761 Paeth H. and Hense A., “SST versus climate change signals in West African rainfall: 20th-
762 century variations and future projections,” *Climatic Change*, vol. 65,no. 1-2, pp. 179–208,
763 2004.
764

765 Paeth H., Girmes R., Menz G., and Hense A., “Improving seasonal forecasting in the low
766 latitudes,” *Monthly Weather Review*, vol. 134, no. 7, pp. 1859–1879, 2006.
767

768 Paeth H, Hall NM, Gaertner MA, Alonso MD, Moumouni S, Polcher J, Ruti PM, Fink AH,
769 Gosset M, Lebel T, Gaye AT, Rowell DP, Moufouma-Okia W, Jacob D, Rockel B, Giorgi F,
770 Rummukainen M. 2011. Progress in regional downscaling of West African precipitation.
771 *Atmos. Sci. Lett.* 12(1): 75–82.
772

773 Pal JS, Small EE, Elthair EA (2000) Simulation of regionalscale water and energy budgets:
774 representation of subgrid cloud and precipitation processes within RegCM. *J Geophys Res*
775 105: 29579–29594
776

777 Pal JS, Giorgi F, Bi X, Elguindi N, Solomon F, Gao X, Francisco R, Zakey A, Winter J,
778 Ashfaq M, Syed F, Bell JL, Diffanbaugh NS, Kamacharya J, Konare A, Martinez D, da Rocha
779 RP, Sloan LC, Steiner A (2007) The ICTP RegCM3 and RegCNET: regional climate
780 modeling for the developing world. *Bull Amer Meteor Soc* 88:1395–1409
781

782 Reynolds RW, Smith TM (1994) Improved global sea surface temperature analysis using
783 optimum interpolation. *J Climate* 7: 929–948
784

785 Simmons AS, Uppala DD, Kobayashi S (2007) ERA-interim: new ECMWF reanalysis
786 products from 1989 onwards. *ECMWF Newsl* 110:29–35
787

788 Singh AP, Singh RP, Raju PVS, Bhatla R. 2011. Comparison of three different cumulus
789 parameterization schemes on Indian summer monsoon circulation. *Int. J. Ocean Clim. Syst.*
790 2(1): 27–43

791
792 Smith SD (1988) Coefficients for sea surface wind stress, heat flux, and wind profiles as a
793 function of wind speed and temperature. *J Geophys Res* 93: 15467–15472
794
795 Soden BJ, Held IM. 2006. An assessment of climate feedbacks in coupled ocean–atmosphere
796 model. *J. Clim.* 19: 3354–3360.
797
798 Solmon F, Giorgi F, Liou C (2006) Aerosol modeling for regional climate studies:
799 application to anthropogenic particles and evaluation over a European/African domain. *Tellus*
800 *Ser B Chem Phys Meteorol* 58:51–72
801
802 Srinivas CV, Hariprasad D, Rao DVB, Anjaneyulu Y, Baskaran R, Venkataraman B. 2013.
803 Simulation of the Indian summer monsoon regional climate using advanced research WRF
804 model. *Int. J. Climatol.* 33: 1195–1210.
805
806 Steiner, A., J. Pal, S. Rauscher, J. Bell, N. Diffenbaugh, A. Boone, L. Sloan, et al., 2009.
807 “Land Surface Coupling in Regional Climate Simulations of the West African Monsoon.”
808 *Climate Dynamics* 33: 869–892.
809
810 Sultan B, Janicot S. 2000. Abrupt shift of the ITCZ over West Africa and intra-seasonal
811 variability. *Geophysical Research Letters* 27:3353–3356.
812
813 Sultan, B., Janicot, S., & Diedhiou, A. (2003). The West African monsoon dynamics. Part I:
814 Documentation of intraseasonal variability. *Journal of Climate*, 16(21), 3389-3406.
815
816 Sultan B, Janicot S. 2003. The West African monsoon dynamics. Part II: The “preonset” and
817 “onset” of the summer monsoon. *J. Climate* 16(21): 3407–3427.
818
819 Sundqvist HE, Berge E, Kristjansson JE (1989) The effects of domain choice on summer
820 precipitation simulation and sensitivity in a regional climate model. *J Climate* 11: 2698–2712
821
822 Sylla MB, Gaye AT, Pal JS, Jenkins GS, Bi XQ. 2009. High resolution simulations of West
823 Africa climate using Regional Climate Model (RegCM3) with different lateral boundary
824 conditions. *Theor. Appl. Climatol.* 98(3–4): 293–314, DOI: 10.1007/s00704-009-0110-4.

825
826 Sylla MB, Giorgi F, Ruti PM, Calmanti S, Dell'Aquila A. 2011. The impact of deep
827 convection on the West African summer monsoon climate: a regional climate model
828 sensitivity study. *Q. J. Roy. Meteorol. Soc.* 137: 1417–1430, DOI: 10.1002/qj.853.
829
830 Sylla MB, Giorgi F, Stordal F. 2012. Large-scale origins of rainfall and temperature bias in
831 high resolution simulations over Southern Africa. *Climate Res.* 52: 193–211, DOI:
832 10.3354/cr01044.
833
834 Sylla MB, Giorgi F, Coppola E, Mariotti L (2013a) Uncertainties in daily rainfall over Africa:
835 assessment of observation products and evaluation of a regional climate model simulation. *Int*
836 *J Climatol.* doi:10.1002/joc.3551
837
838 Sylla MB, Diallo I, Pal JS., 2013b. West African monsoon in state of the art regional climate
839 models. In *Climate Variability Regional and Thematic Patterns*, Tarhule A (ed). ISBN: 980-
840 953-307-816-3.
841
842 Tadross MA, Gutowski WJ Jr, Hewitson BC, Jack C, New M. 2006. MM5 simulations of
843 interannual change and the diurnal cycle of
844 southern African regional climate. *Theor. Appl. Climatol.* 86(1–4): 63–80.
845
846 Thorncroft CD, Blackburn M (1999) Maintenance of the African easterly jet. *Q J R Meteorol*
847 *Soc* 125:763–786
848
849 Tiedtke, M. 1989. “A Comprehensive Mass Flux Scheme for Cumulus Parameterization in
850 Large-scale Models.” *Monthly Weather Review* 117: 1779–1800.
851
852 Uppala S, Dee D, Kobayashi S, Berrisford P, Simmons A (2008) Towards a climate data
853 assimilation system: status update of ERA-interim. *ECMWF Newsl* 115:12–18
854
855 Wang, G., M. Yu, J. S. Pal, R. Mei, G. B. Bonan, S. Levis, and P. E. Thornton (2016), On the
856 development of a coupled regional climate vegetation model RCM-CLM-CN-DV and its
857 validation its tropical Africa, *Clim. Dyn.*, 46, 515–539.
858

859 Xue Y, De Sales F, Lau KMW, Bonne A, Feng J, Dirmeyer P, Guo Z, Kim KM, Kitoh A,
860 Kumar V, Pocard-Leclercq I, Mahowald N, Moufouma-Okia W, Pegion P, Rowell DP,
861 Schemm J, Schulbert S, Sealy A, Thiaw WM, Vintzileos A, Williams SF, Wu ML (2010)
862 Intercomparison of West African Monsoon and its variability in the West African Monsoon
863 Modelling Evaluation Project (WAMME) first model Intercomparison experiment. *Clim Dyn.*
864 doi:10.1007/s00382-010-0778-2

865

866 Zakey AS, Solmon F, Giorgi F (2006) Implementation and testing of a desert dust module in a
867 regional climate model. *Atmos Chem Phys*, 6:4687–4704

868

869 Zaroug MAH, Sylla MB, Giorgi F, Eltahir EAB, Aggarwal PK. 2012. A sensitivity study on
870 the role of the Swamps of Southern Sudan in the summer climate of North Africa using a
871 regional climate model. *Theor. Appl. Climatol.* DOI: 10.1007/s00704-012-0751-6.

872

873 Zeng X, Zhao M, Dickinson RE (1998) Intercomparison of bulk aerodynamic algorithms for
874 the computation of sea surface fluxes using TOGA COARE and TAO DATA. *J Climate* 11:
875 2628–2644

876

877

878

879

880

881

882

883

884

885

886

887

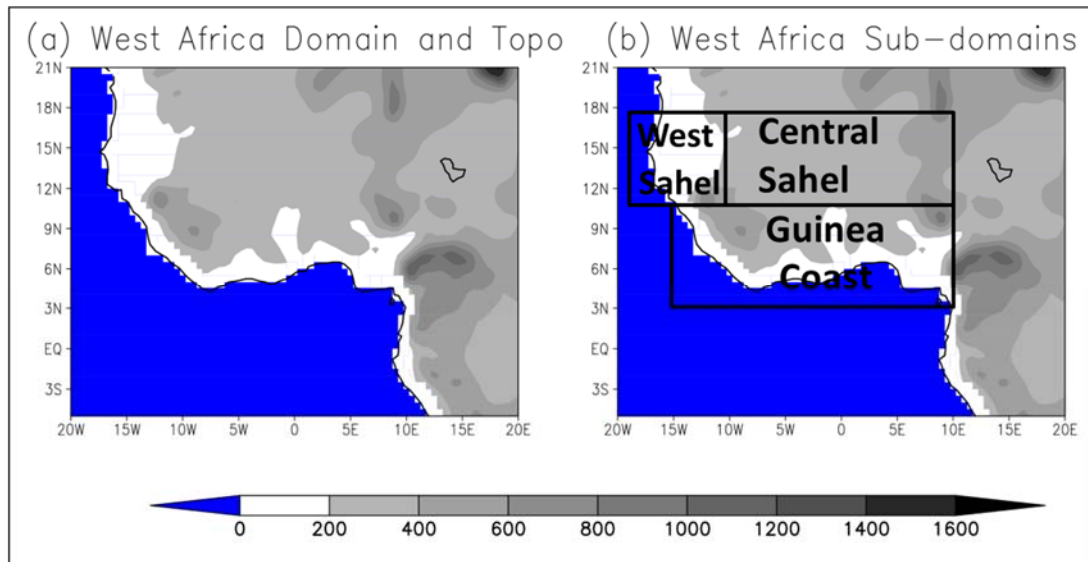
888
 889
 890
 891
 892
 893
 894
 895
 896
 897
 898
 899
 900
 901
 902
 903
 904
 905
 906
 907
 908
 909
 910
 911
 912
 913
 914
 915
 916
 917
 918
 919
 920

	Guinea Coast		Sahel Central		West Sahel		West Africa	
	RMSD (°C)	PCC	RMSD (°C)	PCC	RMSD (°C)	PCC	RMSD (°C)	PCC
UDEL	0.613	0.749	0.475	0.974	0.424	0.981	0.695	0.981
Mix1	1.605	0.768	0.737	0.961	0.720	0.987	1.218	0.978
Emanuel	1.294	0.772	0.673	0.954	0.589	0.986	1.068	0.979
Grell	2.657	0.728	1.406	0.920	1.994	0.985	2.171	0.973
Tiedtke	1.534	0.758	1.360	0.938	0.717	0.982	1.355	0.938
Mix2	1.993	0.781	1.682	0.884	1.568	0.978	1.715	0.964

Table 1: pattern correlation coefficient (PCC) and root mean square difference (RMSD) for JJAS 2m-temperature for model simulations and observation (UDEL) with respect to CRU over sub-regions Guinea Coast, Sahel Central, West Sahel and West Africa domain during the period 2002-2003.

	Guinea Coast	Sahel	West Sahel	West Africa	
	Mean Bias (%)	Mean Bias (%)	Mean Bias (%)	Mean Bias (%)	PCC
TRMM	5	-5.11	4.26	1.24	0.963
Mix1	-18.49	-40.15	-15.07	-22.25	0.719
Emanuel	-27.92	-42.71	-33.56	-25.58	0.807
Grell	-44.29	-56.62	-51.74	-34.07	0.641
Tiedtke	-53.54	-77.14	-56.69	-65.08	0.609
Mix2	-53.44	-50.67	-55.76	-47.66	0.893

Table 2: mean bias (MB) and the pattern correlation coefficient (PCC) for JJAS precipitation for model simulations and observation (TRMM) with respect to GPCP for sub-regions Guinea Coast, Sahel Central, West Sahel and West Africa domain. The PCC is calculated only for the West African domain during the period 2002-2003.



921

922

923

Figure 1: Topography of the West African domain. The analysis of model result is emphasis over the whole West African domain and the three sub-regions Guinea Coast, Sahel Central and West Sahel which are marked with black boxes.

925

926

927

928

929

930

931

932

933

934

935

936

937

938

939

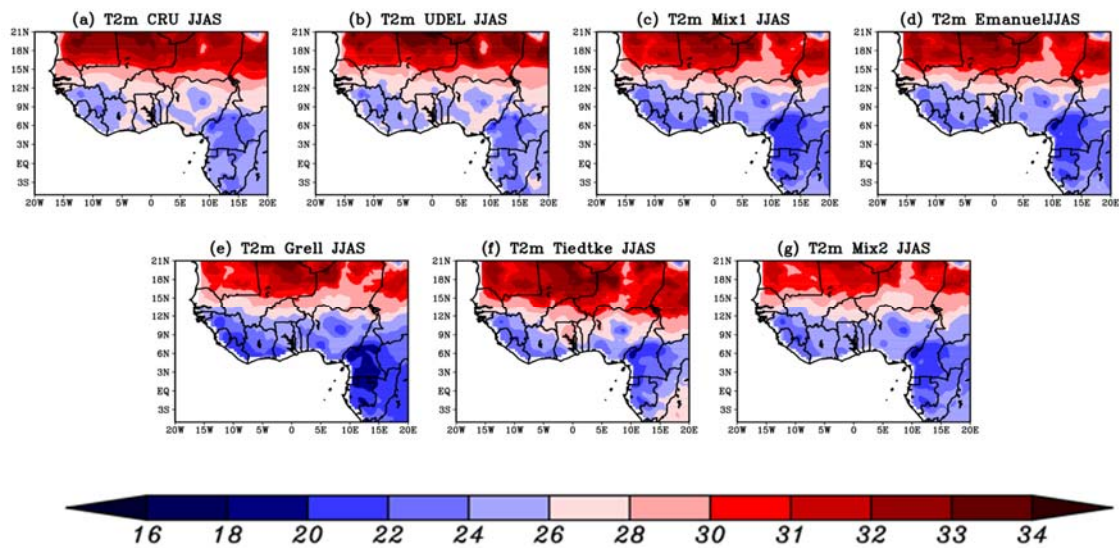
940

941

942

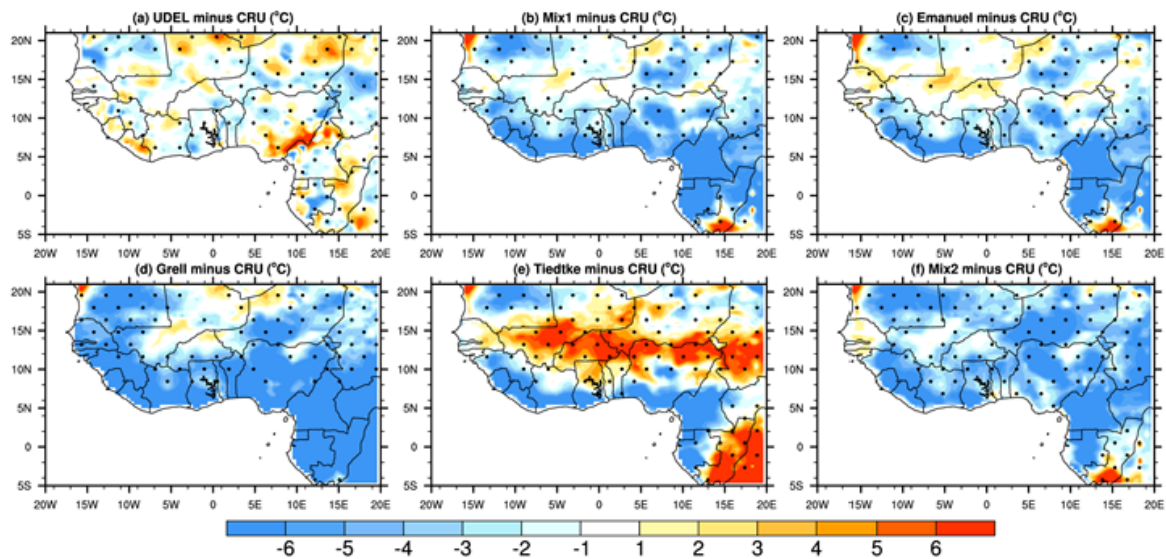
943

944



945
 946
 947
 948
 949
 950
 951
 952
 953
 954
 955
 956
 957
 958
 959
 960
 961

Figure 2: Averaged 2003–2004 JJAS 2m-temperature (in °C) over West Africa from: (a) CRU, (b) UDEL, (c) Mix1, (d) Emanuel, (e) Grell, (f) Tiedtke and (g) Mix2.



962

963

964

965

966

967

968

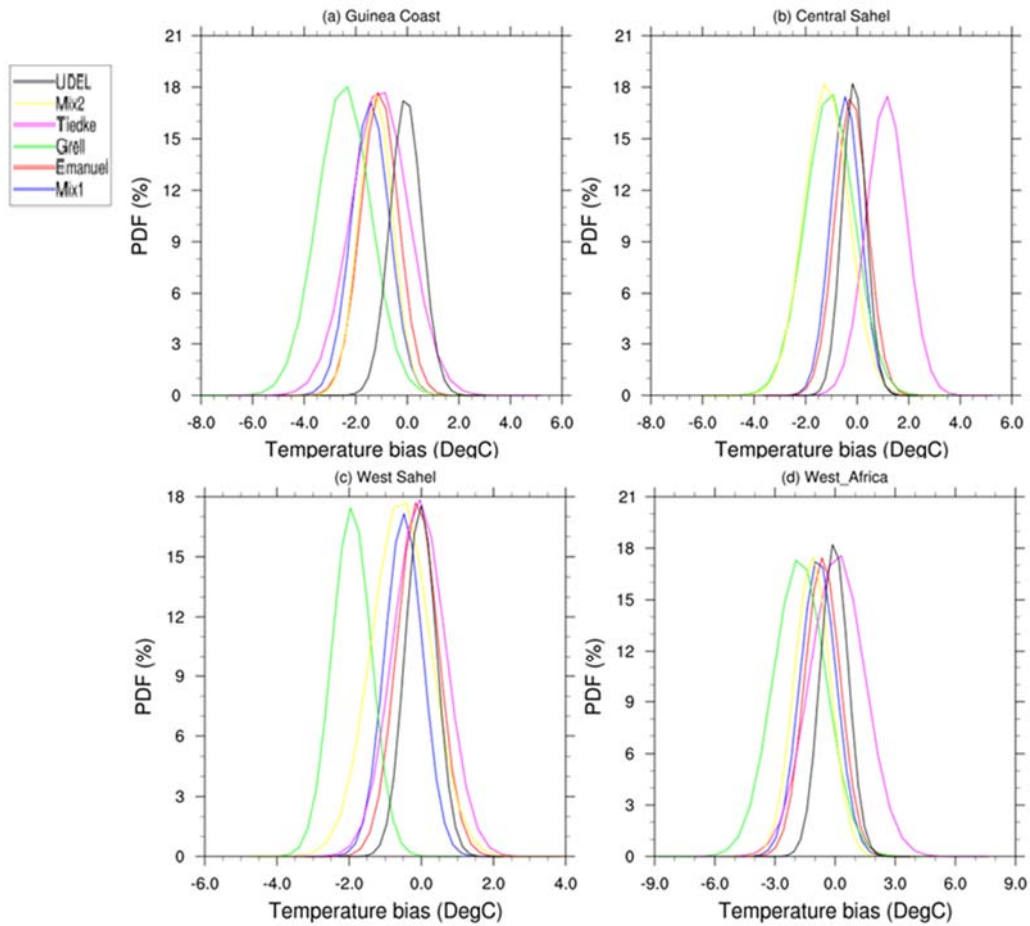
969

970

971

972

Figure 3: JJAS 2m-temperature bias (in °C), over West Africa, with respect to CRU from: (a) UDEL, (b) Mix1, (c) Emanuel, (d) Grell, (e) Tiedtke and (f) Mix2 during the period 2002-2003. The dotted area denotes differences which are statistically significant at a significance level of 0.05.



973

974

975 **Figure 4:** PDF distributions (%) of temperature bias in JJAS over Guinea, Central Sahel,
 976 West Sahel and West Africa, derived from the model simulations using different
 977 convection schemes (land only; units: °C) during the period 2002-2003.

978

979

980

981

982

983

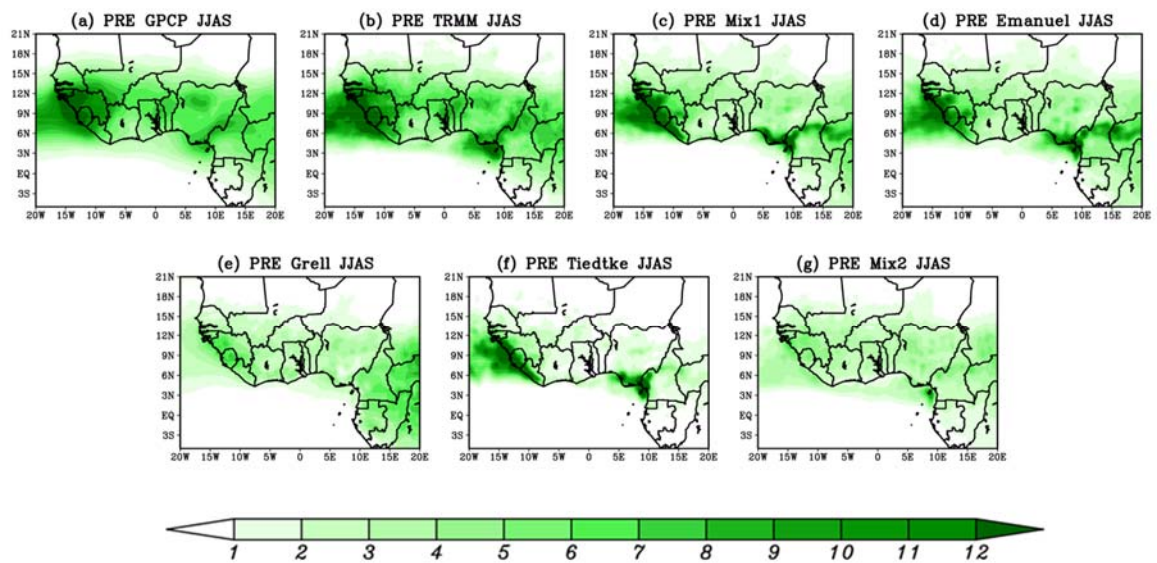
984

985

986

987

988



989

990

991 **Figure 5:** Averaged 2003–2004 JJAS precipitation (in mm/day), over West Africa, from: (a)

992 GPCP, (b) TRMM, (c) Mix1, (d) Emanuel, (e) Grell, (f) Tiedtke and (g) Mix2.

993

994

995

996

997

998

999

1000

1001

1002

1003

1004

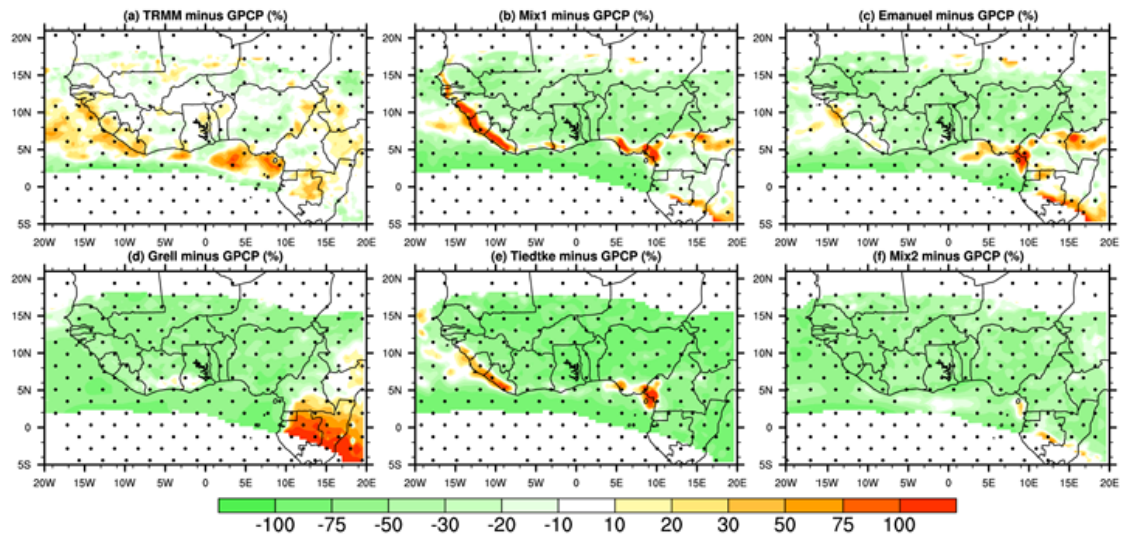
1005

1006

1007

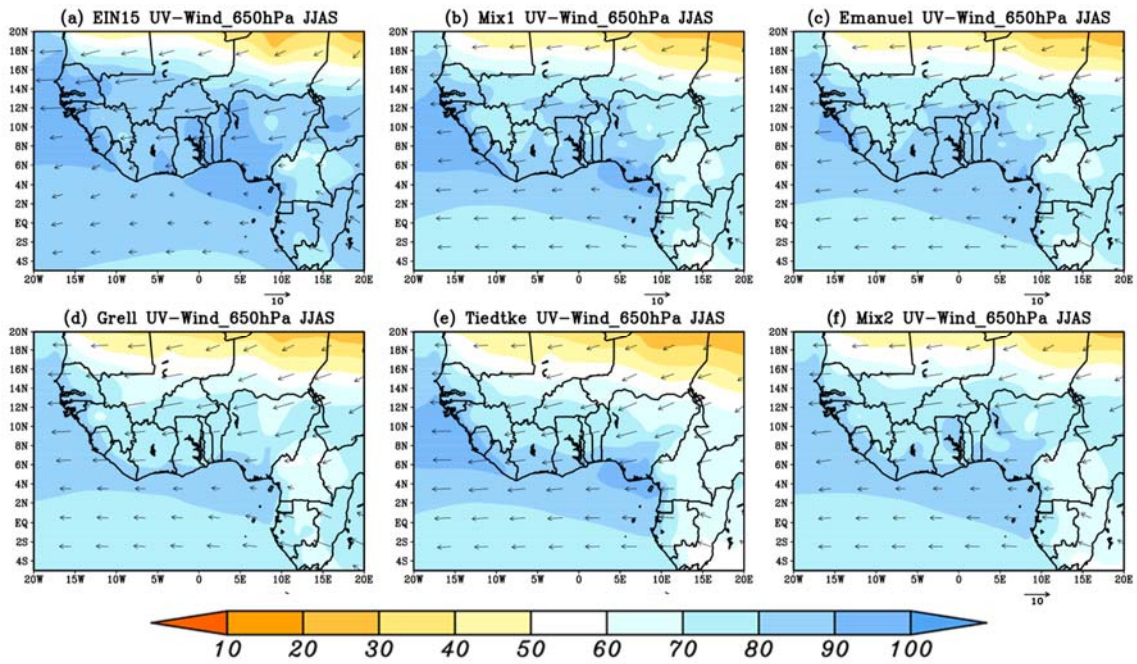
1008

1009



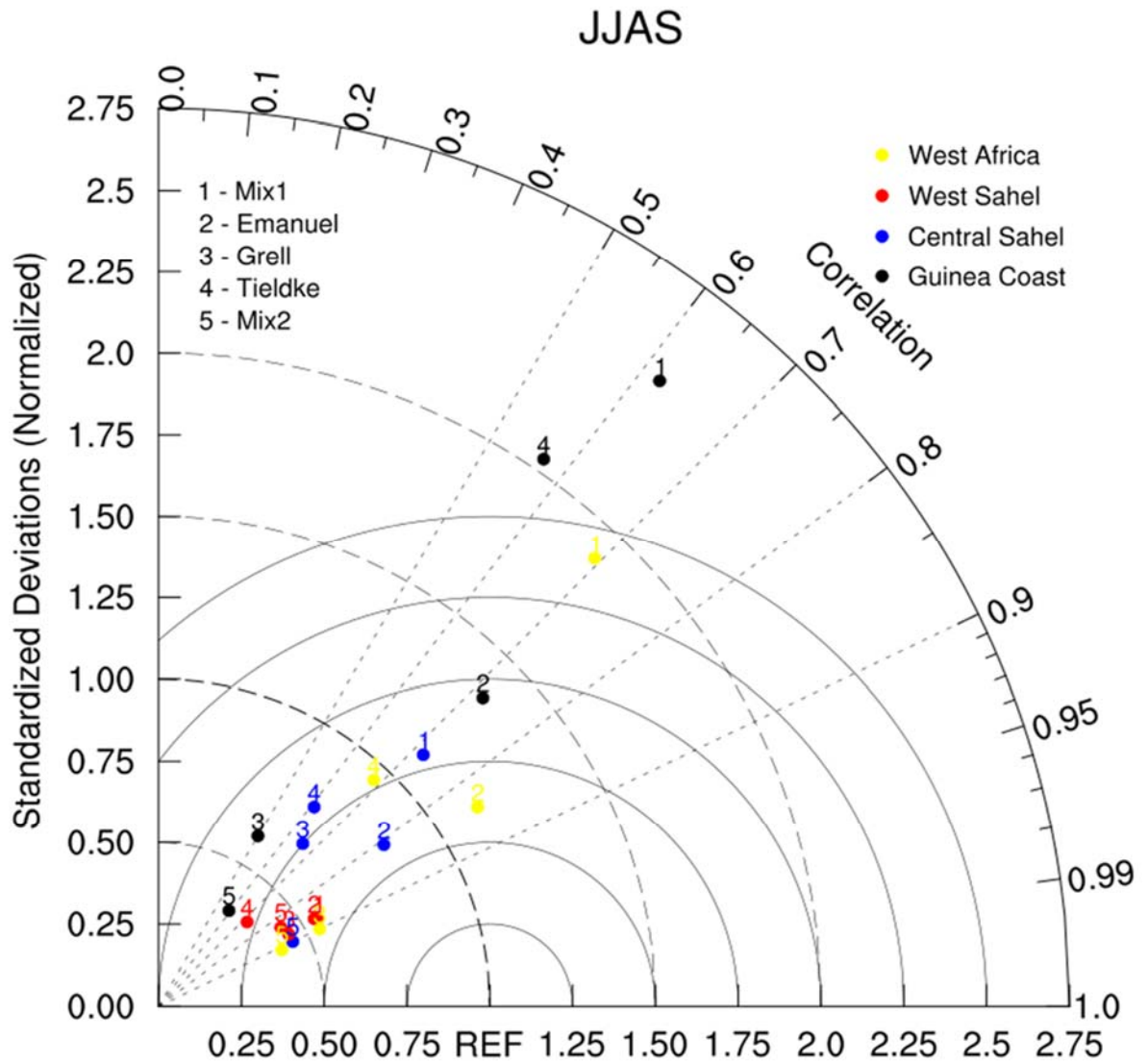
1010
 1011
 1012
 1013
 1014
 1015
 1016
 1017
 1018
 1019
 1020
 1021
 1022
 1023
 1024
 1025
 1026
 1027
 1028
 1029
 1030
 1031

Figure 6: JJAS precipitation bias (in %), over West Africa, with respect to GPCP from :
 (a) TRMM, (b) Mix1, (c) Emanuel, (d) Grell, (e) Tiedtke and (f) Mix2 during the period
 2002-2003.



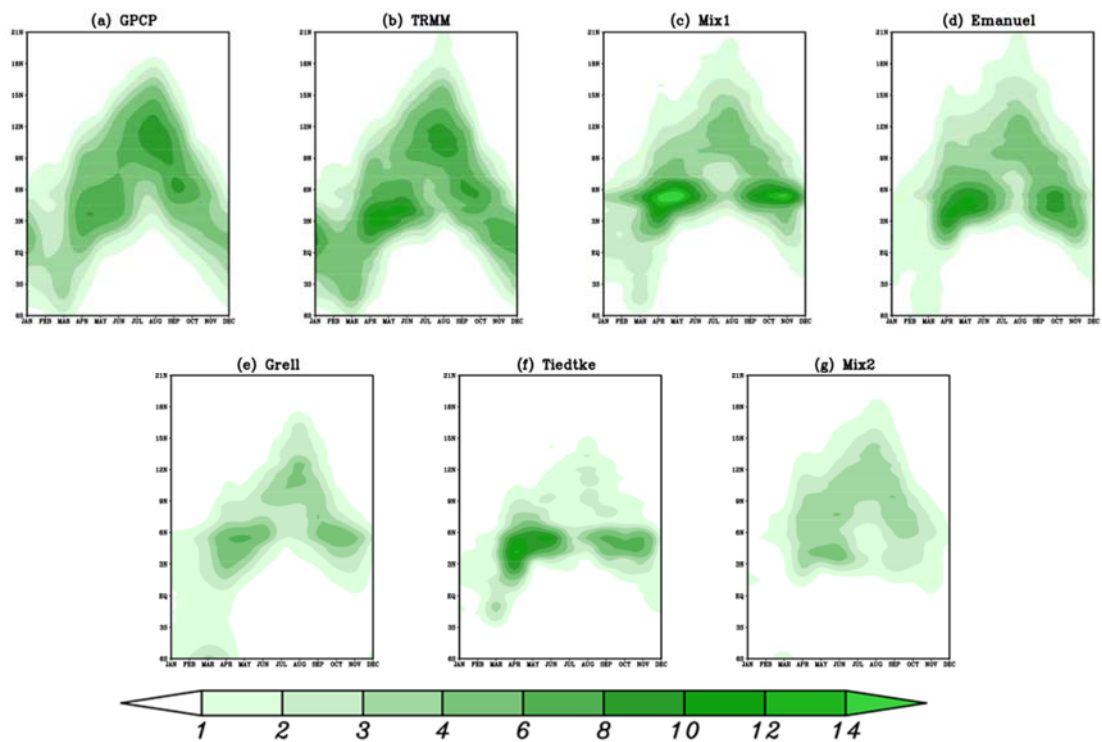
1032
 1033
 1034
 1035
 1036
 1037
 1038
 1039
 1040
 1041
 1042
 1043
 1044
 1045
 1046
 1047
 1048
 1049
 1050
 1051
 1052

Figure 7: The (a) observed and (b–f) simulated vertically mean midlevel (850–300 hPa) integrated specific humidity (shaded) superimposed at zonal winds in JJAS at 650 hPa, over West Africa, from: (a) ERA-Interim, (b) Mix1 (c) Emanuel, (d) Grell (e) Tiedtke and (f) Mix2. Arrows are in m/s and specific humidity is expressed in 10^{-3} kg/kg during the period 2002-2003.



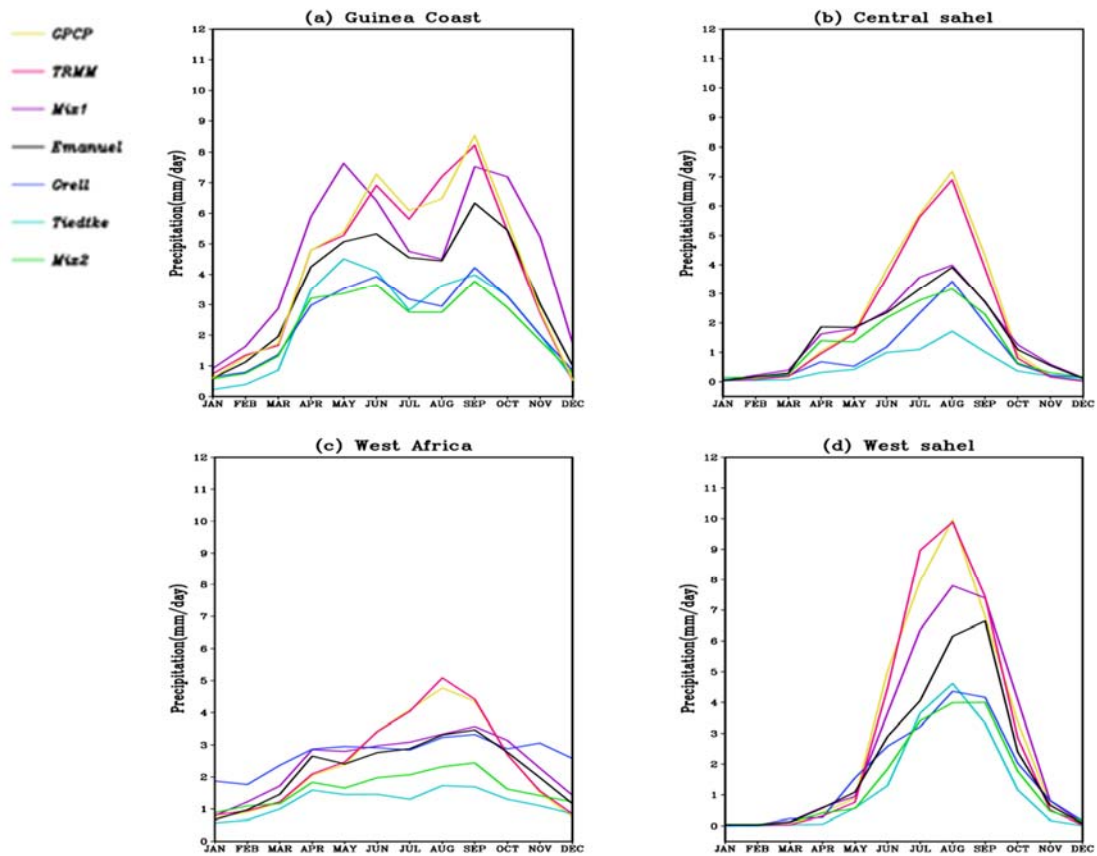
1053
 1054
 1055
 1056
 1057
 1058
 1059
 1060
 1061
 1062

Figure 8: Taylor diagram showing the pattern correlation and the standard deviation (Normalized) for JJAS precipitation with respect to GPCP from: Mix1, Emanuel, Grell, Tiedtke and Mix2 over Guinea Coast, Central Sahel, West Sahel and West Africa during the period 2002-2003.



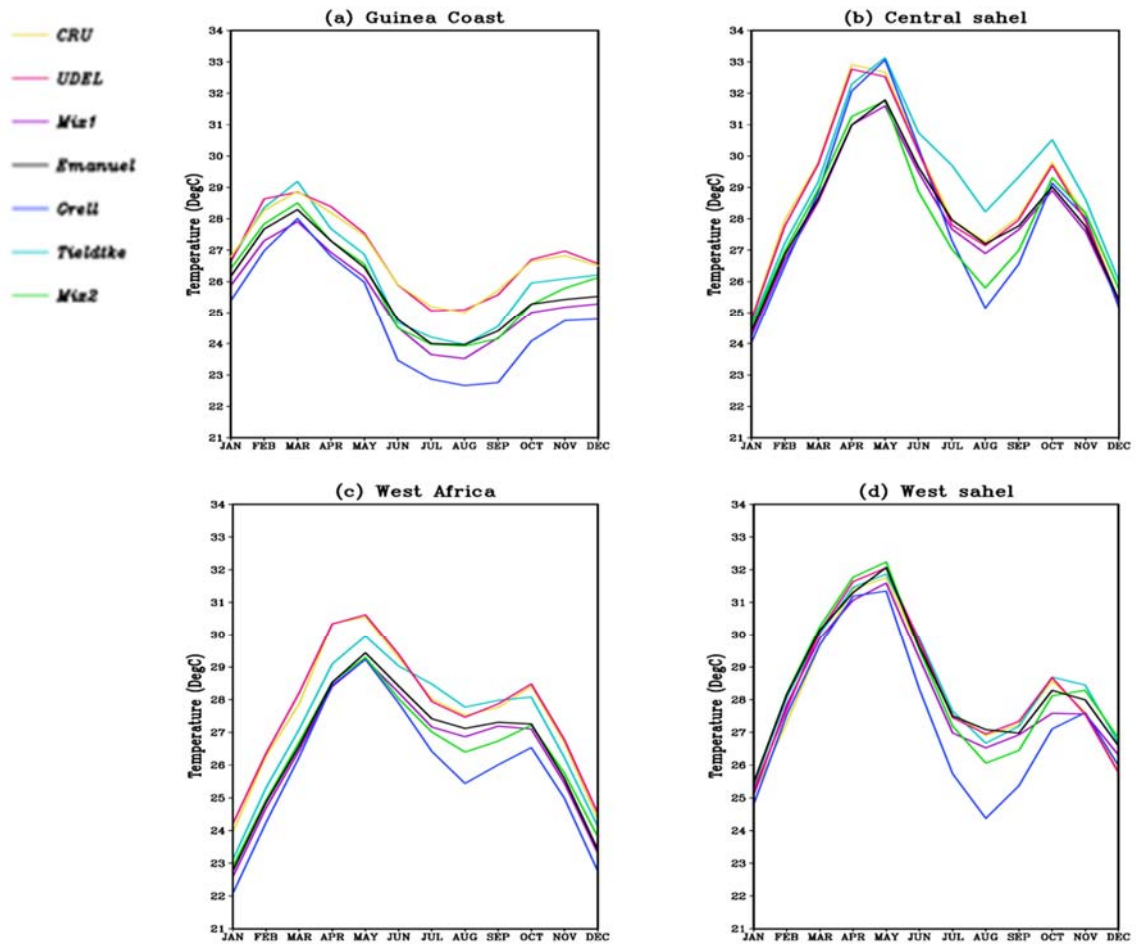
1063
 1064
 1065
 1066
 1067
 1068
 1069
 1070
 1071
 1072
 1073
 1074
 1075
 1076
 1077
 1078
 1079
 1080
 1081
 1082

Figure 9: Hovmoller diagram of monthly precipitation (mm/day) averaged between 10°W and 10°E and for the period 2003-2004 for (a) GPCP, (b) TRMM, (c) Mix1, (d) Emanuel, (e) Grell, (f) Tiedtke and (g) Mix2 under different convective schemes: Mix1, Emanuel, Grell, Tiedtke and Mix2.



1083
 1084
 1085
 1086
 1087
 1088
 1089
 1090
 1091
 1092

Figure 10: Annual cycle of monthly precipitation ($\text{mm}\cdot\text{day}^{-1}$) averaged over, (a) the Guinea Coast West and (b) Central Sahel, (c) West Africa and (d) West Sahel for the period 2003–2004 under different convective schemes: Mix1, Emanuel, Grell, Tiedke and Mix2.



1093

1094

Figure 11: Annual cycle of 2m-Temperature (°C) averaged over, (a) the Guinea Coast, (b) Central Sahel, (c) West Africa and (d) West Sahel for the period 2003–2004 under different convective schemes: Mix1, Emanuel, Grell, Tiedtke and Mix2.

1095

1096

1097

1098

1099

1100

1101

1102

1103

1104

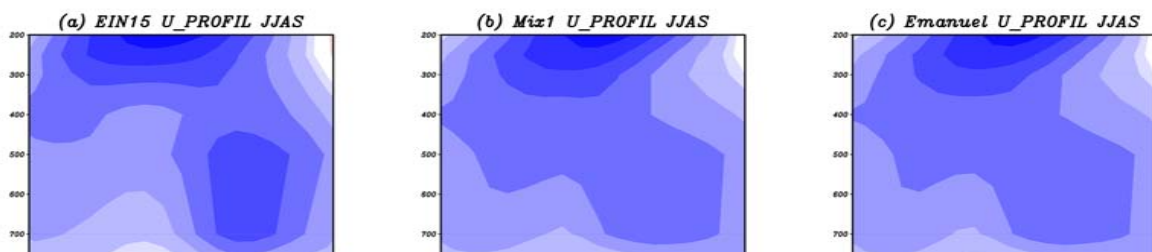
1105

1106

1107

1108

1109



1110
1111
1112
1113
1114
1115
1116
1117
1118
1119
1120
1121
1122
1123
1124
1125
1126
1127
1128
1129

Figure 12: Vertical cross section of the JJAS mean zonal wind (in m/s) averaged between 10°W–10°E, over West Africa, from: (a) ERA-Interim (b) Mix1, (c) Emanuel, (d) Grell, (e) Tiedtke and (f) Mix2. The mean is calculated using the 2003–2004 period.